energies

MDPI

Article

Investigation and Mitigation of Temporary Overvoltage Caused by De-Energization on an Offshore Wind Farm

Ajibola Akinrinde [1,*], Andrew Swanson [2] and Innocent Davidson [1]

[1] Department of Electrical, Power Engineering, Durban University of Technology, Durban 4001, South Africa; innocentd@dut.ac.za

[2] Department of Electrical, Electronics and Computer Engineering, University of KwaZulu-Natal, Durban 4001, South Africa; swanson@ukzn.ac.za

* Correspondence: tunjiakinrinde@yahoo.com

Received: 24 June 2020; Accepted: 19 August 2020; Published: 27 August 2020

Abstract: The Ferranti effect could cause a rise in voltage along the cables on a wind farm if the circuit breakers at the receiving ends are switched off. Ferroresonance could also occur due to stuck pole(s) of the circuit breaker during de-energization. This paper reports on the temporary overvoltage (TOV) arising from the de-energization of the circuit breaker connecting the wind turbine to the feeder, the feeder breaker connecting an array of wind turbines to the point of common coupling (PCC), and the opening of the circuit breaker connecting the onshore to the offshore substation. Ferroresonance was characterized using a phase plane diagram and Poincaré map and was identified to be chaotic. The effect of the nonlinear characteristic of the wind transformer core on the ferroresonant overvoltage was examined and increased with the steepness of slope of the transformer curve. A damping resistor, shunt reactor and surge arrester were used to mitigate the overvoltage experienced during the ferroresonant event. The damping resistor was able to reduce the overvoltage to 1.24 P.U. and damped the ferroresonance from chaotic to fundamental mode.

Keywords: de-energization; Poincaré map; phase plane diagram; wind farm; ferroresonance

1. Introduction

The circuit breaker is a key component in the power system and is used for making circuits during normal operating conditions and breaking them during abnormal situations, being a switching device whose operation is to energize and de-energize an electric circuit. These switching operations could cause stress on the power system by increasing the voltage level of the system, depending on its configuration and the angle at which the circuit breaker is switched. The increase in voltage could either be classified as a temporary or transient overvoltage. If the switching operation includes current chopping, re-ignition, restrike and prestrike, these are regarded as transient overvoltage and are characterized by high voltage spikes. The stress experienced would otherwise be a temporary overvoltage with less magnitude than the transient overvoltage.

Temporary overvoltage is an oscillatory overvoltage between phase-to-phase or phase-to-ground, occurring over a relatively long duration, ranging from seconds to minutes, which is undamped or weakly damped at a frequency equal or close to the power frequency [1]. Temporary overvoltage could occur due to a switching operation circuit breaker or fault clearing event, which includes: load rejection, transformer energization, Ferranti effect, inrush transient, harmonics and ferresonance [2]. Temporary overvoltage (TOV) may have different effects on power systems' equipment, causing high heat in the transformer, and the flashover and breakdown of the insulation. De-energization, being a switching operation, could occur due to the intentional opening of the circuit breaker by the operator,

or unintentionally as a result of a faulty event on the system. De-energization could happen in the form of load rejection, such that the transmission line or the inductive load feeding from the grid is suddenly removed, causing a rise in voltage.

With a 23% growth between 2000 and 2010, and 369.6 GW installed as wind power by the end of 2014 [3], wind energy is now successfully connected to the grid around the world. Investigating possible challenges and proffering solutions is necessary, with challenges including events that could lead to temporary overvoltage. The sudden removal of the load while the wind turbine is operating at full load could lead to an increase in the magnitude of the voltage and power frequency. The overvoltage experienced might not cause instant damage on the power system, but it would cause mechanical stress on the power equipment, gradually degrading the insulation to the level of flashover, thereby exposing it to danger of fast and very fast transient overvoltages.

Various power devices on the offshore wind farm are connected via circuit breakers at each voltage level, the switching operations of these circuit breakers possibly causing overvoltage. The effect of energization events on wind farms that cause both temporary and transient overvoltage have been studied by some researchers, with less emphasis having been placed on de-energization. Some researchers have studied different scenarios of overvoltage on the wind park and considered the entire system [4–11]. Pierrat et al. studied load rejection on a transmission line system with a series capacitor and saturated transformers [4], with the model considering the non-linearity characteristic of the transformer, different levels of load rejection and the asymmetrical operation of the circuit breaker. In [5], Han et al. investigated the effect of transient overvoltages during wind farm switching events on two configurations, these being squirrel cage induction generators and permanent magnet synchronous generators. Liljestrand et al. [6] investigated the transients in a grouped grids of large offshore wind farms with 80 wind turbines, and considered transient events, such as the energization of the feeders and different faults. Badrzadeh et al. [7,8] developed models for the main components of a wind power plant to study transients in a wideband frequency, excluding transformers, which were considered in high frequency. In [9], Chennamadhavuni et al. studied the effect of switching the transient and temporary overvoltage performed on a wind farm, with a wide range of transient events being considered, and the coefficient of grounding (COG) being used to determine the most effective grounding system for the wind farm. King et al. [10] studied the types of switching transients in an array of wind turbines, and considered the level of overvoltage in scenarios of a faulted radial that was both disconnected and connected to the other radials. Ferroresonance in a wind park was studied by Karaagac, where energization and de-energization conditions leading to its occurrence were considered [11].

In this paper, temporary overvoltage caused by the de-energization on an offshore wind farm was investigated. The Ferranti effect causing a voltage rise along the cable due to the symmetrical opening of the circuit breaker was studied, as well as the ferroresonance phenomenon due to the stuck pole(s) of the circuit breaker during de-energization. The circuit breakers considered for de-energization in this study, as shown in Figure 1, were: CB_G at the receiving end of the onshore substation, the feeder breaker A on the medium voltage connecting all wind turbines in a particular row to the PCC, and, lastly, CB_A1 connecting a single DFIG (doubly-fed induction generator) wind turbine. The mode of ferroresonance that existed during the event was determined by characterizing the signal using phase plane and Poincaré map. The influence of the nonlinear characteristic of a transformer core on ferroresonance was also examined, and the best method of mitigation explored.

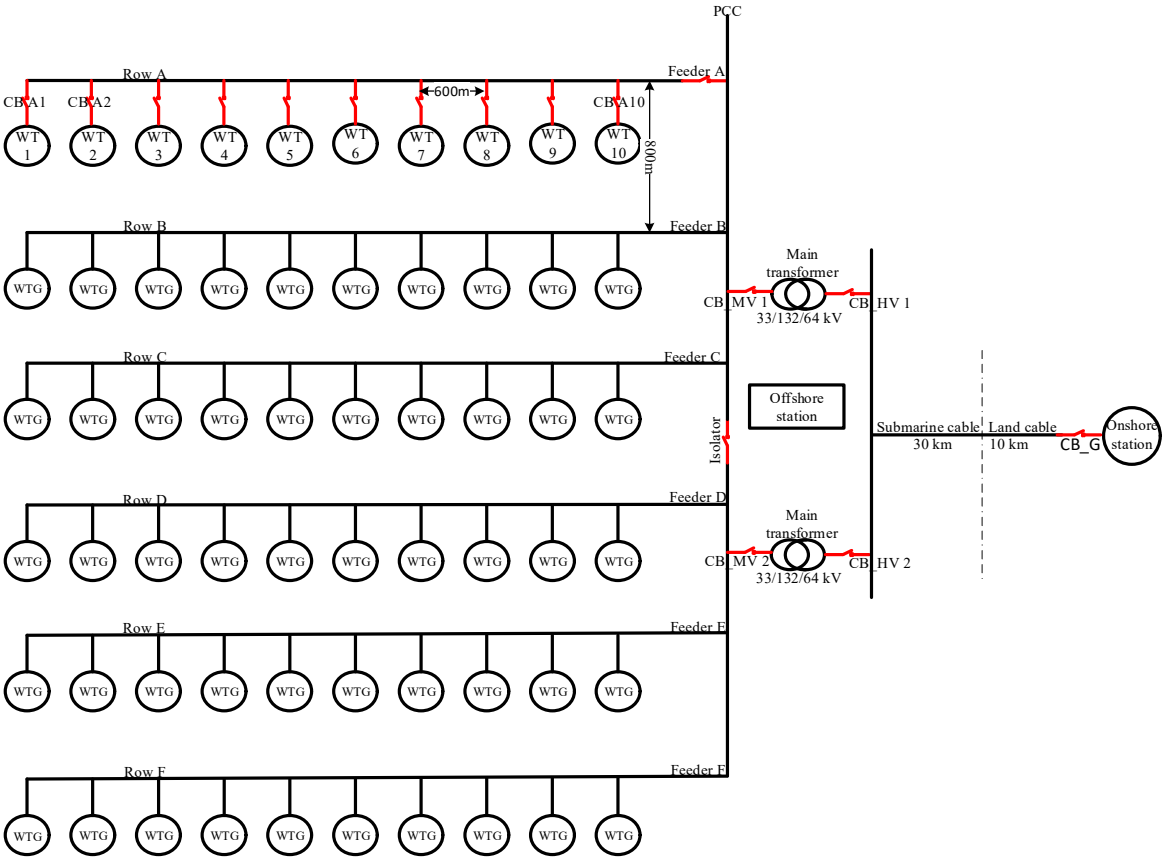

Figure 1. Simplified layout of a wind farm.

2. Modeling

The arrangement of the offshore wind farm examined in this paper consisted of 60 wind turbines in 10 rows and six columns, being connected through 6 feeders to the offshore substation, and finally to the onshore substation that feeds the grid, as shown in Figure 1.

A simplified detail of the wind turbine generator (WTG) shown in Figure 2, which generates 0.69 kV and stepped up by a wind turbine transformer (WTT) rated at 2.5 MVA, 0.69/33/0.69 kV. The main wind farm transformer located on the offshore substation with the rating of 150 MVA, 33/132/64 kV, steps up the voltage to 132 kV, and it is finally transmitted through the submarine and land cable to the onshore substation. According to a report given by the CIGRE Working Group 02 of Study Committee 33, this study could be classified as low frequency transient that falls between 0.1 and 3 kHz [12]. It therefore modeled all the major components on the wind farm, with consideration of the rules guiding low-frequency transients. There are various simulation tools that can be used for electromagnetic transients, but, in this paper, ATP/EMTP was used because it is readily and freely available for all users. ATP/EMTP software is an electromagnetic transients program that can be extensively used for modeling electric complex network and their controls.

2.1. Wind Turbine Model

At the time of writing, the DFIG wind turbine is extensively used on wind farms and appears to be preferred over other types of configurations. This is because they are robust and rugged, allow variable speeds and have the capacity to control both active and reactive power, providing aid to efficient power system dynamics. Thus, the wind turbine was modeled as a DFIG, with the aid of a universal machine (UM4) induction, a tool available on ATP/EMTP software that can be used to model either an induction generator or motor. The wind blade is turned by the kinetic energy of the wind, producing

mechanical energy that is amplified by the gear box to rotate the rotor of the generator. The torque required by the turbine to rotate is given as Equation (1):

$$T_m = \frac{1}{2}\rho A v^3 C_p(\lambda, \beta) \quad (1)$$

where A is the swept area of the turbine blade, ρ is the air density, v is the wind speed and C_p is the power coefficient of the turbine, which is dependent on the pitch angle, β, and the tip speed ratio, λ.

In accordance with the ATP rule book [13], all the mechanical parameters of the turbine, which include aerodynamic torque, angular velocity, inertia, friction coefficient and electromagnetic torque, are represented with electrical parameters as transient analysis of control system (TACS) current source, instantaneous voltage, capacitance, resistance and current source, respectively.

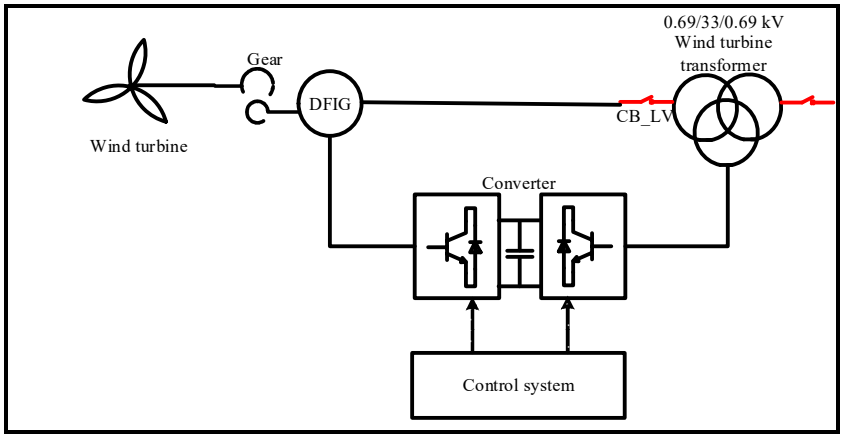

Figure 2. Simplified details of a wind turbine generator.

2.1.1. Modeling of DFIG Wind Turbine Configuration

Modeling the DFIG wind turbine and controlling the back-to-back converter was done according to [14–19]. Table 1 shows the parameters of the DFIG wind turbine.

Table 1. Parameters of the doubly-fed induction generator (DFIG).

Parameters	Values (Ohm)
Rotor inductance	0.033
Rotor resistance	0.0073
stator inductance	0.029
Stator resistance	0.0023
Mutual inductance	0.8436

The operation of DFIG is mathematically explained using the d-q coordinate frame; the a-b-c coordinate axis is converted to the d-q coordinate for all the variables using park's transformation. Equations (2)–(5) depict the stator and rotor voltages of the DFIG, while Equations (6)–(9) depict the fluxes of the stator and rotor. Equations (10) and (11) represent the inductance of the stator and rotor. Thus, Equations (12)–(14) show the electromechanical torque, active power and reactive power of the DFIG generator.

$$V_{sd} = R_s I_{sd} + \frac{d\varphi_{sd}}{dt} - \omega_s \varphi_{sq} \quad (2)$$

$$V_{sq} = R_s I_{sq} + \frac{d\varphi_{sq}}{dt} + \omega_s \varphi_{sd} \quad (3)$$

$$V_{rd} = R_r I_{rd} + \frac{d\varphi_{rd}}{dt} - \omega_r \varphi_{rq} \quad (4)$$

$$V_{rq} = R_r I_{rq} + \frac{d\varphi_{rq}}{dt} + \omega_r \varphi_{rd} \quad (5)$$

$$\varphi_{sd} = L_s I_{sd} + L_m I_{rd} \quad (6)$$

$$\varphi_{sq} = L_s I_{sq} + L_m I_{rq} \quad (7)$$

$$\varphi_{rd} = L_r I_{rd} + L_m I_{sd} \quad (8)$$

$$\varphi_{rq} = L_r I_{rq} + L_m I_{sq} \quad (9)$$

$$L_s = L_{is} + L_m \quad (10)$$

$$L_r = L_{ir} + L_m \quad (11)$$

$$T_e = 1.5\, N_p \frac{L_m}{L_s}\left(I_{sq}\varphi_{sd} - I_{sd}\,\varphi_{sq}\right) \quad (12)$$

$$P_s = \frac{3}{2}\left(V_{sq} I_{sq} + V_{sd}\, I_{sd}\right) \quad (13)$$

$$Q_s = \frac{3}{2}\left(V_{sq} I_{sd} - V_{sd}\, I_{sq}\right) \quad (14)$$

where P_s, T_e, Q_s, N_p are the active power, torque, reactive power and number of poles of the generator, respectively; V_{sd} and V_{sq} are the stator voltages in the d and q axes, respectively; V_{rd} and V_{rq} are the rotor voltages in the d and q axes, respectively; R_s and R_r are the stator and rotor resistance, respectively; L_s and L_r are the stator and rotor inductance, respectively; L_{is} and L_{ir} are the stator and rotor self-inductance, respectively, L_m is the mutual inductance; I_{sd} and I_{sq} are the stator currents in the d and q axes, respectively; I_{rd} and I_{rq} are the rotor currents in the d and q axes, respectively; φ_{sd} and φ_{sq} are the stator fluxes in the d and q axes, respectively, and φ_{rd} and φ_{rq} are the rotor fluxes in the d and q axes, respectively.

2.1.2. Control of Back-to-Back Converter

The back-to-back converter consists of the machine-side converter (MSC), which is a rectifier, and the grid-side converter (GSC), which is an inverter connected via a DC link, with each having six insulator-gated bipolar transistors (IGBTs). They both control the power generated by the generator and the power delivered to the load through the control strategy, as shown in Figure 3. In Figure 3, the MSC control used the maximum power point tracking (MPPT) to regulate the angular velocity and the rotor speed. The result was passed through a PI controller and using Equation (18) to give the reference q-axis rotor current I_{rq} *, which was corrected with the q-axis rotor current I_{rq} and then passed through another controller to give the reference q-axis rotor voltage V_{rqref}. Likewise, the reactive power of the generator Q_s, as expressed in Equation (17), was corrected with a preset value Q_{ref}; the result was passed through a PI controller to give the reference d-axis rotor current I_{rd} *, which was corrected with the d-axis rotor current I_{rd}, and then passed through the controller to give the reference d-axis rotor voltage V_{rdref}. Voltages V_{rdref} and V_{rqref} are compensated using Equations (19) and (20), respectively, to obtain V_{rd} * and V_{rq} *, as expressed in Equations (15) and (16), which were transformed to the a-b-c coordinated axis and finally modulated using a pulse width modulator (PWM).

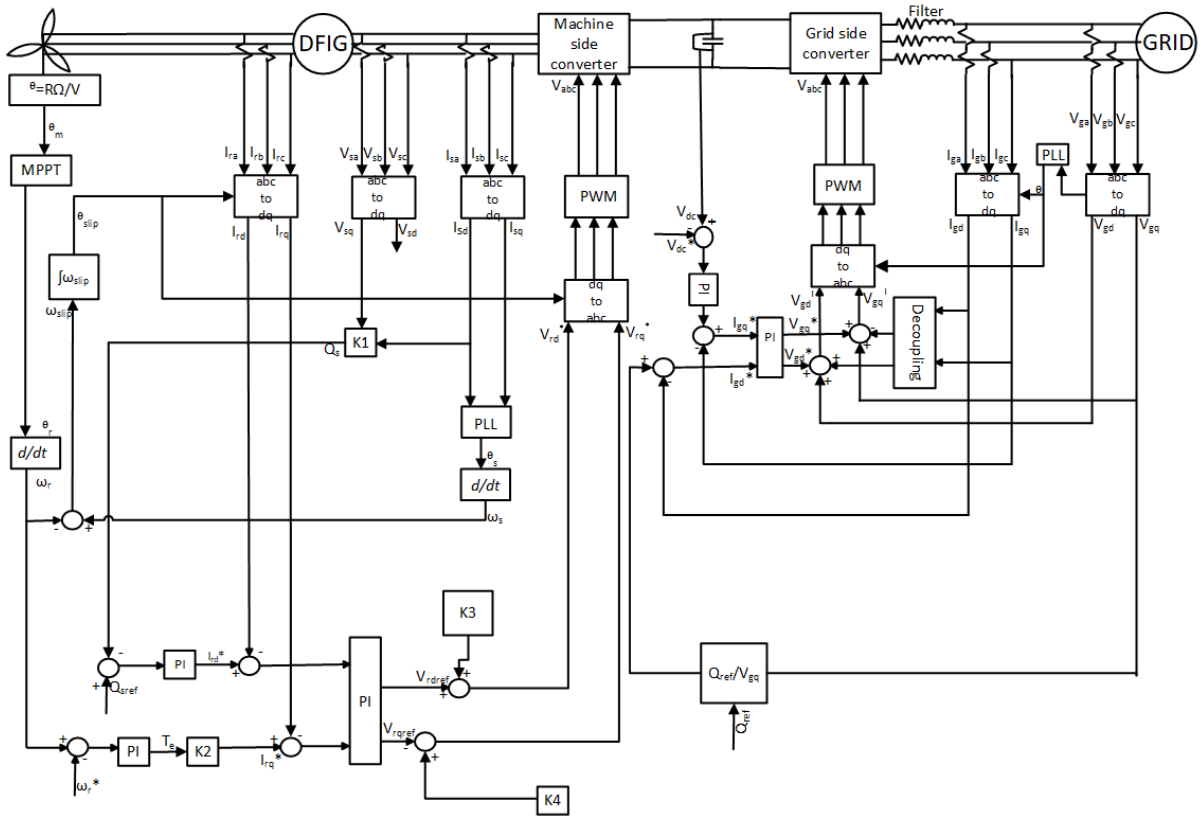

Figure 3. Control scheme of the DFIG generator, including the machine-side converter (MSC) and grid-side converter (GSC).

On the other hand, the GSC control consists of an outer and inner loop. In the outer loop, the voltage of the DC link was corrected with preset voltage and the result was passed through a PI controller to gives the reference q-axis grid current I_{gq} *. The required reactive power by the grid was divided by the q-axis grid voltage V_{gq} and the result was corrected with the d-axis grid current I_{gd} to give reference q-axis grid current I_{gq} *. The inner loop contains a PI controller that converted I_{gq} * and I_{gd} * to reference dq-axis grid voltages V_{gq} * and V_{gd} *, respectively. Voltages V_{gq} * and V_{gd} * are corrected by grid voltages V_{gq} and V_{gd}, respectively, and also decoupled by a low pass filter as shown in Equations (22) and (23). The resultant d-q axis voltages were converted to a-b-c axis while the phase locked loop (PLL) was used to synchronize the voltage and the frequency of the system to the grid and finally passed through the PWM.

$$V_{rd} = I_{rd}R_r + L_r\sigma\frac{dI_{rd}}{dt} - K_3 \tag{15}$$

$$V_{rq} = I_{rq}R_r + L_r\sigma\frac{dI_{rq}}{dt} + K_4 \tag{16}$$

$$k_1 = \frac{1}{2} I_{sd}\, V_{sq} \tag{17}$$

$$k_2 = \frac{L_s\, T_e}{N_p\, \varphi_{sd}\, L_m} \tag{18}$$

$$K_3 = \sigma\omega_r L_r I_{rq} \tag{19}$$

$$K_4 = \omega_r\left(\frac{L_m\varphi_{sd}}{L_s} - \sigma L_r I_{rd}\right) \tag{20}$$

$$\sigma = 1 - \frac{L_m^2}{L_r L_s} \tag{21}$$

$$V_{gd} = V_{sd} + I_{gd}R_g + L_g\frac{dI_{gd}}{dt} - \omega_s L_g I_{gq} \tag{22}$$

$$V_{gq} = V_{sq} + I_{gq}R_g + L_g\frac{dI_{gq}}{dt} + \omega_s L_{gd} \tag{23}$$

where V_{gq} and V_{gd}, are the grid voltages in the q and d axes, respectively, and σ is the dispersion coefficient of the generator.

2.2. Transformers

Both the WTT and the main transformer were modeled using the saturable transformer component (STC) 3-phase model, with the consideration of the non-linearity of the core. The STC model was used to model the WTT in this study and was implemented based on one- and three-phase implementation, which can be obtained by connecting three single phases together. A preset three-phase, three-winding STC model of the WTTs was arranged, with the primary winding is connected to the stator of the generator, while the tertiary winding was connected to the output of the converter. The non-linearity characteristic of the transformers were obtained using the BCTRAN model, which converts the open and short circuit factory test of the transformers to flux–current data, as reported by from Aristi [20]. The resulting positive magnetization curves were extrapolated using a curve fitting tool on Matlab to obtain the full saturation curves. The piecewise nonlinear curves were converted to hysteresis loop using the hysteresis subroutine in the ATP. Table 2 shows the parameters of both the WTTs and main transformer, while Figure 4a,b show the nonlinear curve of the WTT core and main transformer core, respectively, and Figure 5a,b show the hysteresis loop of the WTT core and main transformer core, respectively.

Table 2. Parameters of wind turbine and main transformer.

Transformer	Parameters	Primary	Secondary	Tertiary
Wind turbine transformer	Vector group	D	Y	D
	L (Ω)	0.0327	13.41	0.12
	R (Ω)	0.002	0.42	0.0038
Main transformer	Vector group	Y	Y	D
	L (Ω)	1.88	50.5	118
	R (Ω)	0.057	1.61	3.63

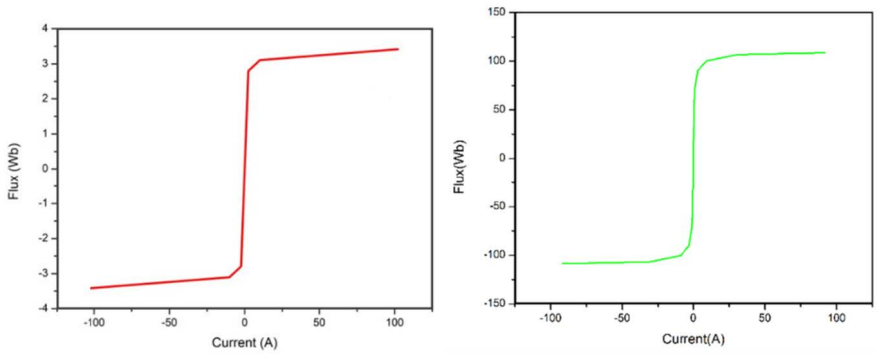

(**a**) (**b**)

Figure 4. Nonlinear curve of transformer cores are as follows: (**a**) WTT core; (**b**) Main transformer core.

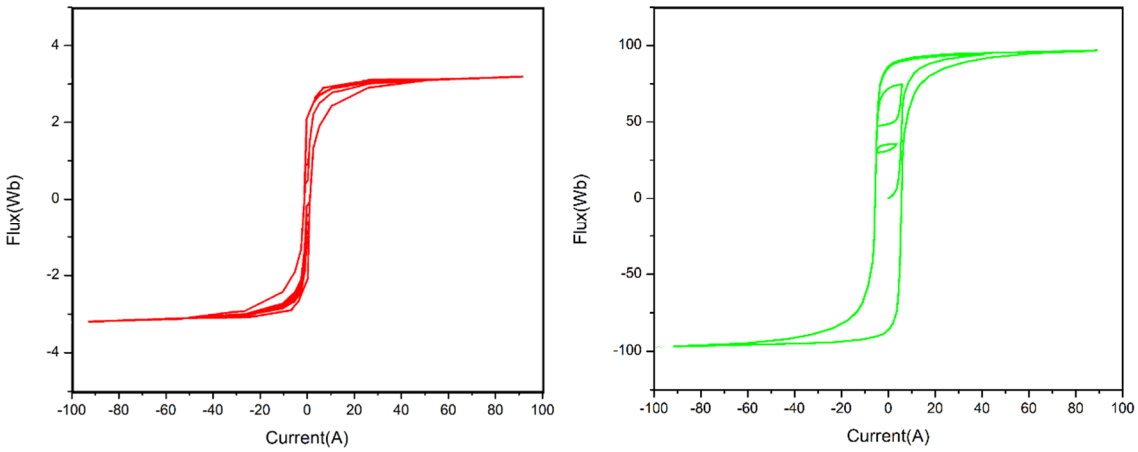

(**a**) (**b**)

Figure 5. Hysteresis loop of transformer cores are as follows: (**a**) wind turbine transformer (WTT) core; (**b**) main transformer core.

2.3. Cables and Circuit Breakers

The length of the cable is very important when considering temporary overvoltage, as the Ferranti effect depends on this distance [4]. A 600 m cable connects one wind turbine to another in a row, while the length of the cable connecting each row to another is 800 m. The offshore substation is connected to the onshore substation via three 630 mm^2 submarine cables and land cables of 30 and 10 km long, respectively. All cables were modeled using the lumped pi model, the data of which were obtained from the data sheet of the manufacturer [21,22].

In accordance with the CIGRE guideline [12], the circuit breaker operation was normal, without considering chopping, restrike and re-ignition, but with temporary overvoltage being considered in this study.

3. De-Energization of One Wind Turbine in a Row

One wind turbine was de-energized from the array of wind turbines on the feeder while others remained closed. Three types of scenarios were evaluated: opening three poles, two poles and one pole of the circuit breaker. These events were evaluated and are discussed in the following subsection.

3.1. Opening of the Three Poles of the Circuit Breaker

The Ferranti effect is common during de-energization at the receiving end of a long transmission line but could also occur when a short cable is de-energized due to the high surge impedance of the cable. The wind turbine A1 is de-energized either due to a fault or maintenance, with all the poles circuit breakers being opened at 0.73 s, when the voltage of one of the phases is at its peak so as to obtain the maximum overvoltage. Figure 6a,b show the overvoltage at the primary and secondary side of the WTT A1. An overvoltage of 5.21 P.U. was observed, which damps toward the steady state over a period of 2.5 s. The effect of de-energizing the CB_A1 on the other wind turbines was examined but were unaffected.

3.2. Opening of the Two Poles of the Circuit Breaker

During de-energization, abnormal operation of the breaker can occur, which can lead to one of the poles being stuck and other two poles opened. This situation could lead to ferroresonance, due to the interaction of the stray capacitance of the submarine cable and the inductance of the WTT. To carry out this event, wind turbine A1 was de-energized with two poles being opened, with Figure 7a,b showing the voltage at the secondary and primary sides of the WTT A1. An overvoltage of 3.88 P.U.

was observed, which remains undamp throughout the simulation time and makes it harmful for the power line equipment, especially the transformer. The effect of ferroresonance that was caused during this event was checked on the other wind turbines on feeder A and found to be unaffected.

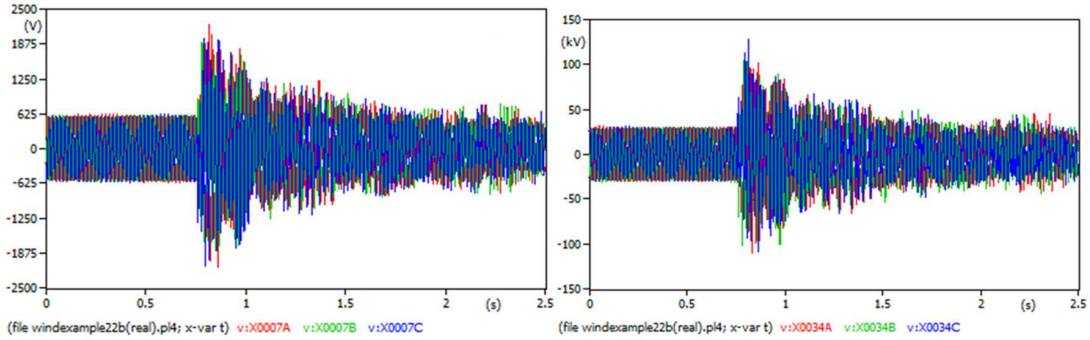

(**a**) (**b**)

Figure 6. Overvoltage at the WTT caused by the opening of three poles are as follows: (**a**) primary side of the WTT; (**b**) secondary side of the WTT.

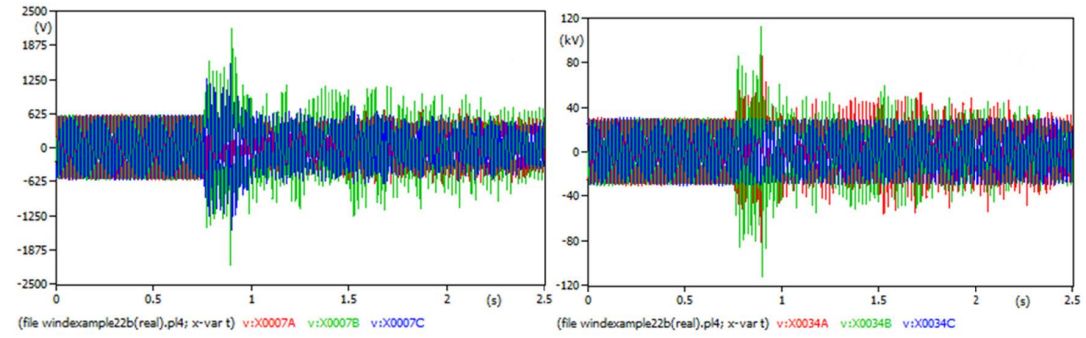

(**a**) (**b**)

Figure 7. Overvoltage at WTT caused by opening of two poles are as follows: (**a**) primary side of the WTT; (**b**) secondary side of the WTT.

3.3. Opening of the One Pole of the Circuit Breaker

Opening one pole would cause the same ferroresonance phenomenon as opening two poles of the breaker. The overvoltage experience due to one pole opening on wind turbine A1 was 1.22 P.U., with the wave form shown in Figure 8a,b for both the high-voltage and primary sides of the A1 WTT, respectively.

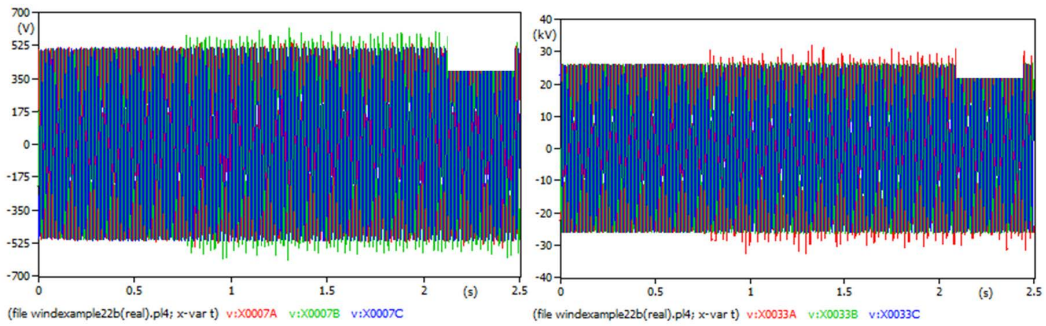

(**a**) (**b**)

Figure 8. Overvoltage at the WTT caused by opening of one pole are as follows: (**a**) primary side of the WTT; (**b**) secondary side of the WTT.

4. De-Energization of Feeder on the MV Bus

In this section, de-energization occurred on the MV bus, with two scenarios being considered that could lead to temporary overvoltage, these being opening one of the incoming and one of the outgoing feeders on the MV bus.

4.1. Opening of One of the Incoming Feeders on the MV Bus

Feeder A was opened at 0.73 s when phase A was at the peak and while all the wind turbines were still operational. The proper opening of all the poles of the feeder had the same overvoltage effect as in Section 3.1 and occurred on all the wind turbines on feeder A. However, this de-energization event did not affect the other feeders on the MV bus.

In the case of ferroresonant conditions, where two and one poles of the feeder A were opened, the same overvoltages as obtained in Sections 3.2 and 3.3 were experienced in the respective events. In each event, the same overvoltage was also experienced on all the wind turbines on feeder A, while the ferroresonance phenomenon was not experienced on other feeders on the MV bus.

4.2. Opening of One of the Outgoing Feeders on the MV Bus

The MV bus arrangement is a single bus bar with sectionalisation, which is used for repairs and maintenance without completely shutting down. Likewise, the arrangement between the MV and the HV bus is parallel, forming a double transmission line system. Ferroresonance in a double transmission line path, which is caused by the interaction of the stray capacitance of the line and bus bar with nonlinear inductance of the transformer, was studied by [23,24].

In this paper, to study the effect of ferroresonance caused by a double transmission path, one of the high-voltage feeders, CB_HV 1, was opened while all other switches remain connected, and the stray capacitance of the bus bar was taken to be 8 nF/m. Ferroresonance was initiated by the nuisance opening of the isolator between feeder C and D at 0.75 s, which resulted in an overvoltage of 1.58 P.U. across all the main transformer 1. Figure 9a,b show the ferroresonant overvoltage experienced on the high and primary sides of the main transformer.

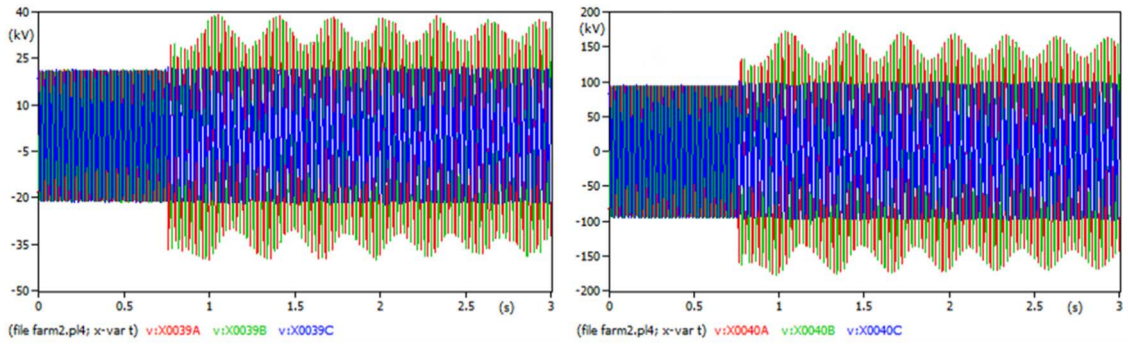

(**a**) (**b**)

Figure 9. Ferroresonant overvoltage at the main transformer 1 caused by double transmission path are as follows: (**a**) primary side; (**b**) secondary side.

5. De-Energization at the Onshore Substation

Three poles' de-energization of the CB_G at the onshore substation occurred, with the resultant waveform for the primary and secondary sides of main transformers being shown in Figure 10a,b, respectively. Overvoltage of 11.14 P.U. was experienced across all the wind turbines during the symmetrical opening of the breaker. Furthermore, a ferroresonance event was simulated by opening two poles of the CB_G. Figure 11a,b are results on the primary and secondary sides of the main

transformers during ferroresonant condition. An overvoltage of 9.34 P.U. was experienced across all the wind turbines due to the ferroresonant condition.

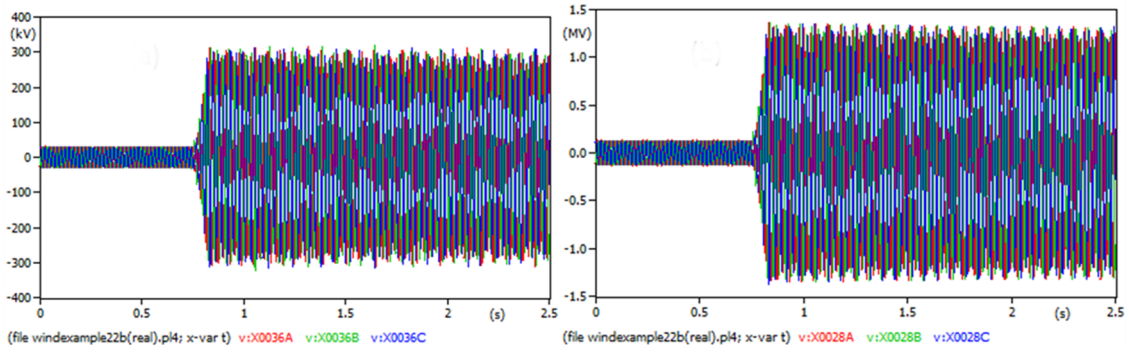

(**a**) (**b**)

Figure 10. Overvoltage at the main transformer due to opening of three poles on the onshore substation are as follows: (**a**) primary side; (**b**) secondary side.

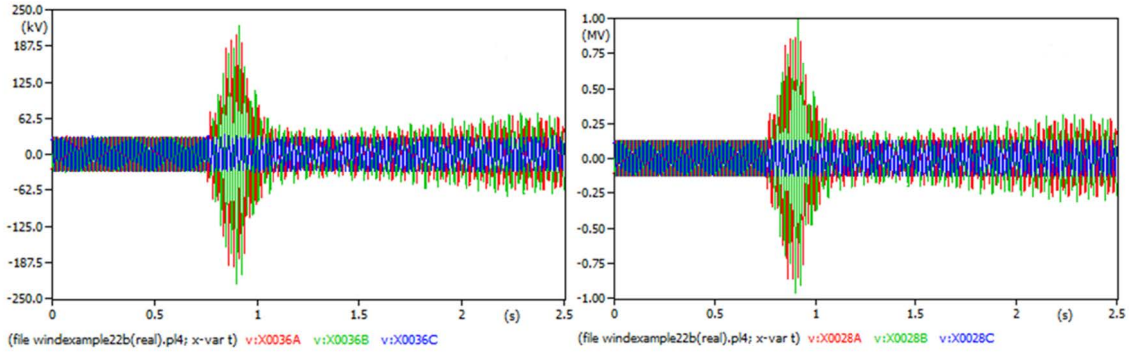

(**a**) (**b**)

Figure 11. Overvoltage the main transformer caused by the opening of two poles leading to ferroresonance: (**a**) primary side; (**b**) secondary side.

6. Influence of Nonlinear Characteristic of the Transformer on Ferroresonant Overvoltage

It was established that ferroresonance occurs in a non-linear circuit, where a non-linear magnetizing inductance interacted with a capacitor. It was therefore expected that change in the nonlinear characteristic of the transformer could cause a sensitive change in the behavior of the system during a ferroresonant event. The inductance was not expected to be linear, due to the saturation of the flux, such that as the current increased so did the magnetic flux, to a point of saturation, where the increase in the current barely has any effect on the increase in the flux. The relationship between the magnetizing current and the flux linkage is expressed in Equation (24):

$$I = a\lambda + b\lambda^n \tag{24}$$

where λ is the flux linkage, I is the magnetizing current, a and b are the coefficients of the linear and saturated region of the curve, respectively, and n is the degree order of the saturation, which is always an odd integer.

To obtain the degree order of saturation "n", and the constant coefficients (a and b) of the nonlinear curve of the WTT, the nonlinear curve fitting tool of Matlab was used. Isqcurvefit is an optimization tool that can solve a nonlinear curve fitting problem in the least square sense and can find the coefficients

that best fit the equation of the function. Equation (25) determines the coefficients of X that best fits the objective function to the Y_{data}, solving it in a least square sense.

$$X = \text{Isqcurvefit}(\text{fun}, X_0, X_{data}, Y_{data}) \quad (25)$$

where X_{data} is the input data, X_0 is the starting point of X_{data}, Y_{data} is the observed output data and fun is the objective function that estimates the value of X. Hence, Isqcurvefit was applied to the data set of Figure 4a. The influence of the nonlinear characteristic of the WTT during the ferroresonant event on one of the wind turbines was examined. To do this, wind turbine A1 was de-enegized as one pole of the breaker was stuck and the other poles were opened, while other turbines remained closed. The nonlinearity was altercated by varying the parameters of Equation (24), as shown in Table 3, leading to nonlinear curves, as shown in Figure 12.

Table 3. Coefficients for different WTT curves.

a	b	n
1.1558	0.0694	5
0.5149	0.0088	7
0.2680	0.00094	9
0.1811	0.0000985	11

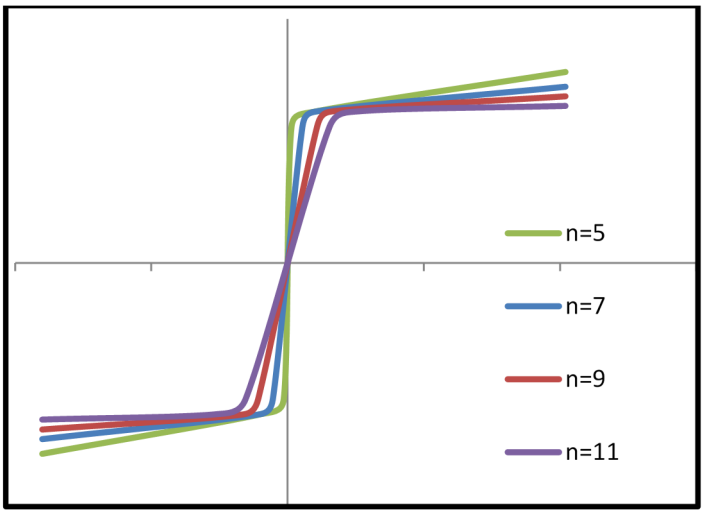

Figure 12. Nonlinear curves of the WTT core with different degree order of saturation.

Wind turbine A1 was de-energized with two poles opened and using the core curve of WTT with parameters a = 1.1558, b = 0.0694 and n = 5, the resultant waveform being shown in Figure 13.

Further analysis was done using phase plane diagram and Poincaré map in order to characterize the mode of ferroresonance that existed in the system. Figure 14a,b are the phase plane diagram and Poincaré map of the overvoltage obtained in Figure 13, and these depict that a chaotic mode of ferroresonance exists in the system due to the erratic behavior, their frequency not following any periodic orbit. The chaotic mode ferroresonance also existed in the WTT when other core curves were investigated using their parameters, as shown in Table 3. However, there was an increase in the chaotic mode and overvoltage experience, the overvoltage with increasing degrees of saturation being show in Table 4.

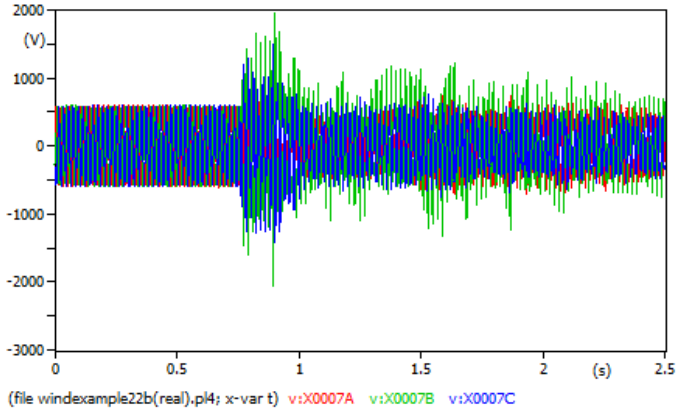

Figure 13. Ferroresonant overvoltage experienced at the primary side of the WTT of A1 when n = 5.

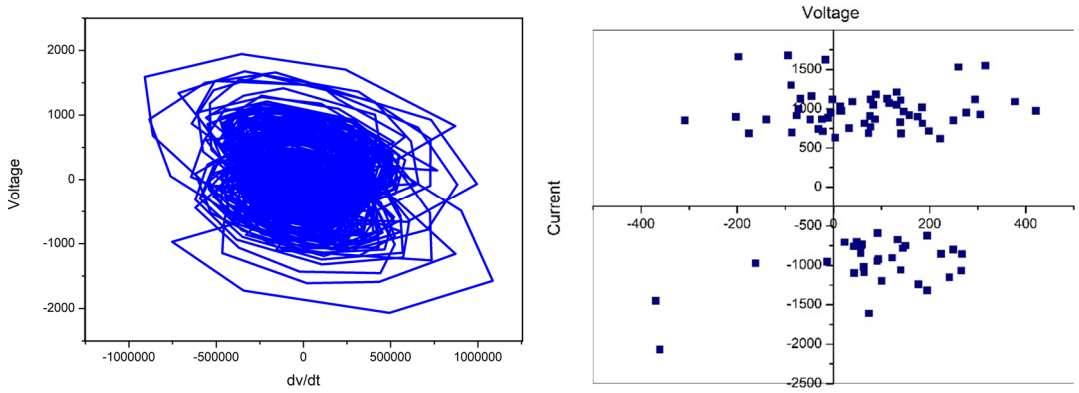

(**a**) (**b**)

Figure 14. Characterization of ferrorsonant waveform when n = 5, depicting chaotic ferroresonance mode are as follows: (**a**) phase plane diagram; (**b**) Poincaré map.

Table 4. Overvoltage of different wind turbine curve.

a	b	n	Overvoltage (PU)
1.1558	0.0694	5	3.77
0.5149	0.0088	7	3.88
0.2680	0.00094	9	4.12
0.1811	0.0000985	11	4.33

7. Mitigation of Overvoltage

It is necessary to mitigate temporary overvoltage, especially when it is above the rated basic insulation level (BIL) of the power system [25], with the tolerable temporary overvoltage being 2 P.U. [1]. However, the overvoltages investigated in this paper were above the BIL and remained undamped, requiring mitigation methods to be considered, and included damping resistors, surge arresters and shunt reactors. These methods were used to suppress the ferroresonance experienced on the WTT during the opening of two poles of the breaker.

7.1. Use of Damping Resistor

A damping resistor is connected across the circuit breaker for the purpose of damping and reducing the overvoltage [25]. The damping resistor used for mitigation was approximately 40 Ω, which was calculated using Equation (26):

$$\frac{3\sqrt{3}V_n^2}{P_e} \tag{26}$$

where V_n is the nominal voltage of the winding and P_e the thermal limit burden of the transformer, which is the power a transformer can function at without an excessive rise in temperature.

The effect of the damping resistor can be seen in Figure 15a, with the overvoltage observed at the primary side of the WTT being reduced to 1.24 PU. While the chaotic ferroresonance mode no longer existed, the fundamental harmonic ferroresonance mode did continue to exist in the system, as shown by the phase plane diagram in Figure 15b. A single periodic orbit in the phase plane depicts the fundamental harmonic ferroresonance mode.

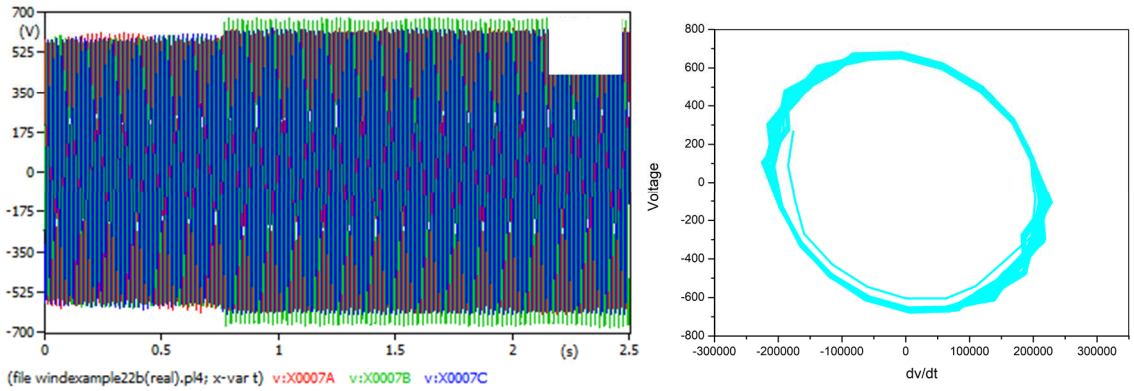

(**a**) (**b**)

Figure 15. Suppression of ferroresonance at the primary side of the WTT using damping resistor are as follows: (**a**) Voltage waveform; (**b**) Phase plane depicting fundamental harmonic ferroresonance mode.

7.2. Use of Shunt Reactor

A shunt reactor was connected close to the transformer, with the reactor being calculated using Equations (27)–(29):

$$R = \frac{1}{\omega C} \tag{27}$$

$$C = \frac{1}{\omega^2 L} \tag{28}$$

$$L = \frac{1}{\omega^2 C} \tag{29}$$

The parameters of the reactor are given as R = 5 Ω, C = 636.54 μF, and L = 16 mH, and by using the reactor, the ferroresonant overvoltage was reduced to 1.78 PU, as shown in Figure 16a. However, Figure 16b shows the phase plane diagram of the Figure 16a, which depicts a reduction in the chaotic mode.

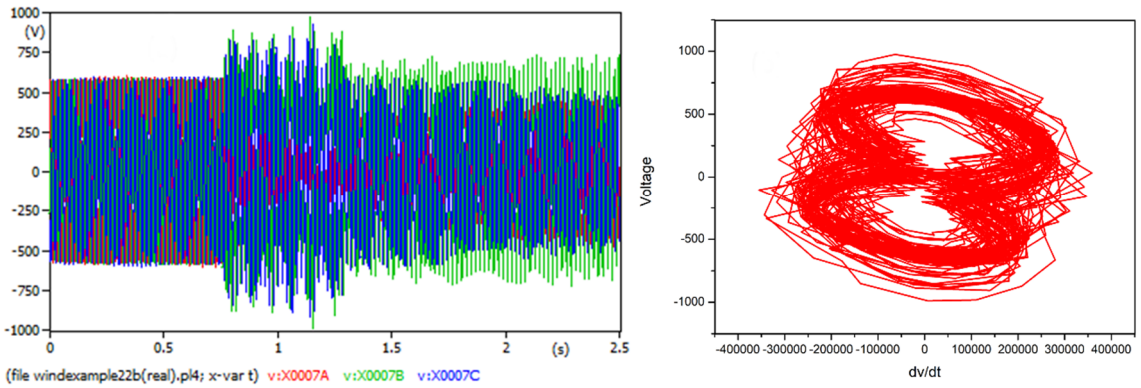

(**a**) (**b**)

Figure 16. Suppression of ferroresonance at the primary side of the WTT using shunt reactor are as follows: (**a**) voltage waveform; (**b**) phase plane depicting chaotic ferroresonance mode.

7.3. Use of Surge Arrester

Surge arresters are not designed to limit the TOV but the fast and very fast transient overvoltages, which could be damaged by the TOV. The choice of surge arrester depends on the maximum continuous operating voltage (MCOV) and rated voltage. There are diverse models of surge arrester, these include and are not limited to the institute of electrical and electronics engineers (IEEE), Pinceti, Fernandez and WR models. The surge arrester in this study was modeled using the IEEE model, because other models are derived from it and the V-I characteristic of the non-linear resistors were obtained according to the IEEEANSI C62.11-1993 standard [26]. The data used to model the surge arrester were presented by the manufacturer in [27], where the residual voltage value for the current impulse of 10 kA, 80/20 µs and the height of the arrester were obtained to be 98 kV and 694 mm, respectively. Overvoltage was reduced to 1.51 P.U. with the use of surge arrester, as shown in Figure 17a, whereby the system became less chaotic, as depicted by phase plane diagram in Figure 17b.

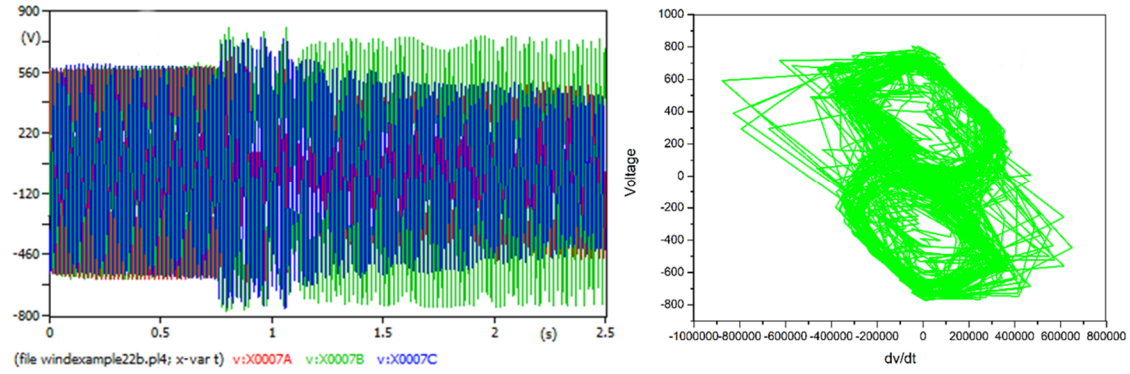

(**a**) (**b**)

Figure 17. Suppression of ferroresonance at the primary side of the WTT using surge arrester are as follows: (**a**) voltage waveform; (**b**) phase plane depicting chaotic ferroresonance mode.

8. Conclusions

This paper investigated the temporary overvoltage due to de-energization on a wind farm. Overvoltage was experienced when the circuit breaker CB_A1 connecting wind turbine A1 to the array of wind turbine was de-energized. Three, two and one pole of the circuit breaker were opened and overvoltages of 5.21, 3.88, and 1.22 P.U. were observed, respectively. Ferroresonance occurs during opening of one and two pole(s) of the breaker, and the overvoltage remained undamped for the

simulation time. Only the de-energized wind turbine was affected by these overvoltages, while other wind turbines were working in their normal condition. However, during the de-energization of feeder A, all the wind turbines on this feeder experienced the same overvoltages as a result of the de-energization of CB_A1, while the other feeders remained unaffected.

Ferroresonance on the double transmission lines was recorded as 1.45 P.U., which was caused by the opening of one of the outgoing feeders on the MV bus. A circuit breaker connecting the offshore to the onshore substation was opened symmetrically, with the resulting overvoltage being approximately about 11.14 P.U.; this was due to the Ferranti effect, which rises through the long submarine and land cables and occurred at distance of 67 km. However, an overvoltage of 9.34 P.U. was observed due to ferroresonance when one of the circuit breaker poles became stuck, which was caused by the interaction of the high capacitance of the cable and the saturated transformer. Ferroresonance on the WTT was characterized using a phase plane diagram and Poincaré map, and found to be a chaotic mode of ferroresonance. The influence of the nonlinear curve of the core on the ferroresonance was examined, with the slope of the curve getting steeper, which may have caused and increase in overvoltage. Mitigating methods for correcting ferroresonant overvoltage caused by opening two poles of the circuit breaker CB_A1 were analyzed. The use of a damping resistor was found to be the most effective method, reducing the overvoltage to 1.24 P.U. and damped the ferroresonance from chaotic to fundamental mode. Meanwhile, a shunt reactor and surge arrester reduced the overvoltage to 1.78 and 1.51 P.U., respectively, but the ferroresonance remained chaotic because both mitigation measures could not damp the overvoltage. Overall, this paper shows that events of de-energization on a wind farm could cause overvoltage higher than the rated BIL level of the power devices on the system. This is more devastating in an event of ferroresonance, which was found to be chaotic in this study. Thus, this study recommended the use of a damping resistor among other correcting measures to be highly effective for the mitigation of ferroresonance.

Author Contributions: This article is part of work of A.A. and it is being supervised by A.S. A.A. did the following in the manuscript; conceptual frame work, simulation on ATP/EMTP, matlab and write up as well. A.S. and I.D. were responsible for editing and technical correction of the manuscript, as well as sourcing for the article processing charge. All authors have read and agreed to the published version of the manuscript.

Funding: This research received no external funding.

Conflicts of Interest: There is no conflict of interest among authors.

References

1. IEC 60071-1. *Insulation Co-ordination-Part1: Definitions, Principles and Rules*; International Electrotechnical Commission: Geneva, Switzerland, 2006; p. 67.
2. IEEE Draft Guide for the Application of Neutral Grounding in Electrical Utility Systems, Part IV—Distribution. In *IEEE PC62.92.4/D6.2, September 2014*; IEEE: Piscataway, NJ, USA, 2014; pp. 1–38.
3. Global Wind Energy Council. 2014 Marked a Record Year for Global Wind Power 2013. Available online: http://www.gwec.net/global-figures/wind-energy-global-status/ (accessed on 5 February 2020).
4. Pierrat, L.; Tran-Quoc, T.; Lam-Du, S. Overvoltages following load rejection on a system with a series-compensated transmission line and saturated transformers. In Proceedings of the 8th Mediterranean Electrotechnical Conference on Industrial Applications in Power Systems, Computer Science and Telecommunications (MELECON 96), Bari, Italy, 16 May 1996.
5. Han, C.; Martin, D.E.; Lezama, M.R. Transient Over-Voltage (TOV) and its suppression for a large wind farm utility interconnection. In Proceedings of the 2009 International Conference on Sustainable Power Generation and Supply, Nanjing, China, 6–7 April 2009.
6. Liljestrand, L.; Sannino, A.; Breder, H.; Thorburn, S. Transients in collection grids of large offshore wind parks. *Wind Energy Int. J. Prog. Appl. Wind Power Convers. Technol.* **2008**, *11*, 45–61. [CrossRef]
7. Badrzadeh, B.; Hogdahl, M.; Isabegovic, E. Transients in Wind Power Plants—Part I: Modeling Methodology and Validation. *IEEE Trans. Ind. Appl.* **2012**, *48*, 794–807.

8. Badrzadeh, B.; Zamastil, M.H.; Singh, N.K.; Breder, H.; Srivastava, K.; Reza, M. Transients in Wind Power Plants; Part II: Case Studies. *IEEE Trans. Ind. Appl.* **2012**, *48*, 1628–1638.
9. Chennamadhavuni, A.; Munji, K.K.; Bhimasingu, R. Investigation of transient and temporary overvoltages in a wind farm. Power System Technology (POWERCON). In Proceedings of the 2012 IEEE International Conference on Power System Technology (POWERCON), Auckland, New Zealand, 30 October–2 November 2012.
10. King, R.; Moore, F.; Jenkins, N.; Haddad, A.; Griffiths, H.; Osborne, M. Switching transients in offshore wind farms–impact on the offshore and onshore networks. In *International Conference on Power Systems Transients*; IPST: Delft, The Netherlands, 2011.
11. Karaagac, U.; Mahseredjian, J.; Cai, L. Ferroresonance conditions in wind parks. *Electr. Power Syst. Res.* **2016**, *138*, 41–49. [CrossRef]
12. Cigre. *Guidelines for Representation of Network Elements When Calculating Transients*; Cigre Technical Brochure: Paris, France, 1990.
13. Prikler, L.; Høidalen, H.K. *ATPdraw Version 5.6 for Windows 9x/NT/2000/XP/Vista-Users' Manual*; European EMTP ATP Users Group: Main, Germany, 2009.
14. Jedut, L.; Rosolowski, E.; Nayir, A. Modeling and control of wind turbine. In Proceedings of the 6th International Conference on Technical and Physical Problems of Power Engineering (ICTPE), Tabriz, Iran, 14–16 September 2010.
15. Nayir, A.; Rosolowski, E.; Jedut, L. Modeling and control of wind turbine and fault. In Proceedings of the 7th International Conference on Technical and Physical Problems of Engineering (ICTPE), Lefkosa, Northern Cyprus, 7–9 July 2011.
16. Nayir, A.; Rosolowski, E.; Jedut, L. Analysis of short circuit faults in a system fed by wind turbine. In Proceedings of the 2012 International Conference on R enewable Energy Research and Applications (ICRERA), Nagasaki, Japan, 11–14 November 2012.
17. Calzolari, G.; Saldana, C. Modeling of Doubly Fed Induction Machine Based Wind Turbine in ATP: Challenges and experiences. In Proceedings of the International Conference on Power Systems Transients (IPST), Vancouver, BC, Canada, 18–20 July 2013.
18. Akinrinde, A.; Swanson, A.; Tiako, R. Dynamic behavior of wind turbine generator configurations during ferroresonant conditions. *Energies* **2019**, *12*, 639. [CrossRef]
19. Akinrinde, A.O.; Swanson, A.; Tiako, R. Effect of ferroresonance on wind turbine: Comparison of ATP/EMTP and matlab/simulink. *Indones. J. Electr. Eng. Comput. Sci.* **2019**, *14*, 1581–1594. [CrossRef]
20. Aristi, I.A. Modeling of Switching Transients in Nysted Offshore Wind Farm and Its Comparison with Measurements: EMT Simulations with Power Factory and PSCAD. Master's Thesis, Technical University of Denmark, DTU, Lyngby, Denmark, 2008.
21. ABB. *XLPE Submarine Cable Systems-Attachment to XLPE Submarine Cable Systems-Users Guide*; ABB's High-Voltage Cable Unit; ABB: Stockholm, Sweden, 2010.
22. ABB. *Submarine Cable Systems-Attachment to XLPE Land Cable Systems-Users Guide*; ABB's High-Voltage Cable Unit; ABB: Stockholm, Sweden, 2010.
23. Charalambous, C.; Wang, Z.; Osborne, M.; Jarman, P. Sensitivity studies on power transformer ferroresonance of a 400 kV double circuit. *IET Gener. Transm. Distrib.* **2008**, *2*, 159–166. [CrossRef]
24. Ang, S.P.; Wang, Z. Ferroresonance Simulation Studies of Transmission Systems. Ph.D. Thesis, University of Manchester, Manchester, UK, 2010.
25. Akinrinde, A.O.; Swanson, A.; Tiako, R. Investigation and Analysis of Temporary Overvoltages Caused by Filter Banks at Onshore Wind Farm Substation. *Int. J. Renew. Energy Res. (IJRER)* **2017**, *7*, 770–777.
26. *IEEE Standard for Metal-Oxide Surge Arresters for AC Power Circuits (>1 kV)*; IEEE Std C62.11-2012 (Revision of IEEE Std C62.11-2005); IEEE: Piscataway, NJ, USA, 2012; p. 121.
27. ABB. *Data sheet Surge Arrester Polim-D, PI-3 Outdoor*; ABB: Wettingen, Switzerland, 2013; p. 4.